

FRAGMENTATION OF MAGNETICALLY SUBCRITICAL CLOUDS INTO MULTIPLE SUPERCRITICAL CORES AND THE FORMATION OF SMALL STELLAR GROUPS

ZHI-YUN LI

Department of Astronomy, University of Virginia, P.O. Box 3818, Charlottesville, VA 22903;
z14h@virginia.edu

AND

FUMITAKA NAKAMURA

Faculty of Education and Human Sciences, Niigata University, 8050 Ikarashi-2, Niigata 950-2181, Japan, and
Astronomy Department, University of California at Berkeley, Berkeley, CA 94720

Draft version November 14, 2018

ABSTRACT

Isolated low-mass stars are formed in dense cores of molecular clouds. In the standard picture, the cores are envisioned to condense out of strongly magnetized clouds through ambipolar diffusion. Most previous calculations based on this scenario are limited to axisymmetric cloud evolution leading to a single core, which collapses to form an isolated star or stellar system at the center. These calculations are here extended to the nonaxisymmetric case under thin-disk approximation, which allows for a detailed investigation into the process of fragmentation, fundamental to binary, multiple system, and cluster formation. We have shown previously that initially axisymmetric, magnetically subcritical clouds with an $m = 2$ density perturbation of modest fractional amplitude ($\sim 5\%$) can develop highly elongated bars, which facilitate binary and multiple system formation. In this paper, we show that in the presence of higher order ($m \geq 3$) perturbations of similar amplitude such clouds are capable of breaking up into a set of discrete dense cores. These multiple cores are magnetically supercritical. They are expected to collapse into single stars or stellar systems individually and, collectively, to form a small stellar group. Our calculations demonstrate that the standard scenario for single star formation involving magnetically subcritical clouds and ambipolar diffusion can readily produce more than one star, provided that the cloud mass is well above the Jeans limit and relatively uniformly distributed. The fragments develop in the central part of the cloud, after the region has become magnetically supercritical but before rapid collapse sets in. It is enhanced by the flattening of mass distribution along the field lines and by the magnetic tension force, which is strong enough during the subcritical-to-supercritical transition to balance out the gravity to a large extent and thus lengthen the time for perturbations to grow and fragments to separate out from the background.

Subject headings: binaries: formation — ISM: clouds — ISM: magnetic fields — MHD — stars: formation

1. INTRODUCTION

Dense cores of molecular clouds play a pivotal role in star formation (Myers 1999). They provide a crucial link between the molecular clouds and the stars formed in them. In the standard picture for isolated low-mass star formation, the cores are envisioned to gradually condense out of a magnetically subcritical background cloud, through ambipolar diffusion (Shu, Adams & Lizano 1987; Mouschovias & Ciolek 1999; see Nakano 1998 and Myers 1999 for an alternative view involving turbulence decay). Detailed calculations based on this scenario have been carried out by many authors (e.g., Nakano 1979; Lizano & Shu 1989; Ciolek & Mouschovias 1993; Basu & Mouschovias 1994). It has been established that prior to star formation dense cores have (1) a central region of flat density distribution surrounded by a roughly r^{-2} envelope, (2) an infall speed over an extended region that could be a significant fraction of the isothermal sound speed, and (3) a field strength typically half the critical value. All these features are consistent with the observations of L1544 (Tafalla et al. 1998; Ward-Thompson et al. 1999; Crutcher & Troland 2000), arguably the best studied starless core (e.g., Caselli et al. 2002). Ambipolar diffusion-driven cloud evolution

models computed specifically for this source (without explicit treatment of turbulence) can match quantitatively its observed mass distribution, velocity field and magnetic field strength (Ciolek & Basu 2000), and plausibly the abundances and spatial distributions of various commonly-observed molecular species, such as CO, N_2H^+ , and CCS, as well (Li et al. 2002). For L1544, the standard scenario appears to provide a reasonable description (see Crutcher et al. 1994 for the successful application of a similar model to the dark cloud B1, for which the field strength is also measured).

Most calculations based on the standard scenario are axisymmetric. As such, they can not directly address the fundamental issue of cloud fragmentation, which lies at the heart of binary, multiple stellar system and cluster formation (Bodenheimer et al. 2000). Indeed, there has been some nagging concern whether a magnetic field strong enough to provide most of the cloud support would at the same time prevent fragmentation (Galli et al. 2001). This is certainly the case if the field is completely frozen in the matter (Nakano 1988). Even a somewhat weaker frozen-in field which does not prevent a cloud from collapsing dynamically may stifle fragmentation (Dorfi 1982;

Phillips 1986a,b). However, these results have limited applicability to molecular clouds, which are only lightly ionized and partially coupled to the magnetic field. For a lightly ionized medium of uniform density threaded by a uniform magnetic field, Langer (1978) showed through linear analysis that the criterion for gravitational instability is unaffected by the field, although the growth rate can be. For a strongly magnetized dark cloud, the instability grows on an ambipolar diffusion time scale, which is typically an order of magnitude longer than the dynamic time. Non-linear developments of this magnetically-mediated gravitational instability in molecular clouds have not been explored in any detail (see Indebetouw & Zweibel 2000 for simulations of a related instability). How or even whether they can lead to cloud fragmentation into discrete pieces capable of forming more than one star remains uncertain. It is the focus of our investigation.

There is some indication that a strong magnetic field may actually promote molecular cloud fragmentation. Boss (2002) followed the evolution of a set of initially magnetically supported clouds in three dimensions (3D), taking into account several magnetic effects approximately. He concluded that the cloud fragmentation is enhanced by magnetic fields because the magnetic tension helps to prevent a central density singularity from forming and producing a dominant single object. Li (2001) studied the 1D evolution of a set of flattened, magnetically subcritical clouds assuming axisymmetry and found that either a dense supercritical core or off-centered ring forms as a result of ambipolar diffusion. Nakamura & Li (2002) showed through 2D nonaxisymmetric calculations that the core-forming clouds are unstable to the $m = 2$ nonaxisymmetric mode, with density perturbations of modest fractional amplitude ($\sim 5\%$) growing nonlinearly into bars of a typical aspect ratio ~ 2 during the transition period after the core has just become supercritical (which makes the bar growth possible) but before rapid collapse sets in (which leaves little time for further growth). They found that, by the time the isothermal approximation starts to break down, the elongation has been strongly amplified by the Lin-Mestel-Shu (1965) instability, producing highly elongated bars. These bars are expected to break up gravitationally into pieces during the subsequent adiabatic phase of evolution, which could lead to the formation of binary and multiple stellar systems. The possible bar fragmentation into multiple systems will be explored elsewhere. Here, we concentrate on the evolution of nonaxisymmetrically perturbed, ring-forming clouds which, as we show in the paper, are capable of producing a number of discrete, magnetically supercritical cores while still in the isothermal phase of cloud evolution. Even though we cannot follow the evolution of the cores beyond the isothermal phase, we anticipate each of them to collapse individually into a single star or stellar system and, collectively, to form a stellar group or small cluster.

We describe our formulation of the problem of magnetic cloud evolution and fragmentation, including the governing equations, initial conditions, and numerical methods in § 2. This is followed by a set of representative models illustrating the main features of nonaxisymmetric cloud evolution leading to fragmentation (§ 3). In the last section (§ 4), we discuss the nature of magnetic cloud fragmenta-

tion, comment on the implications of our calculations on stellar group formation, and conclude.

2. FORMULATION OF THE PROBLEM

2.1. Basic Equations

We consider nonaxisymmetric evolution of strongly magnetized molecular clouds driven by ambipolar diffusion, as envisioned in the standard picture of low-mass star formation. The strong magnetic field allows the cloud material to settle along field lines into a disk-like geometry, maintaining vertical force balance even during the dynamic collapse phase of cloud evolution (Fiedler & Mouschovias 1993). We adopt the standard thin-disk approximation (e.g., Ciolek & Mouschovias 1993; Basu & Mouschovias 1994; Shu & Li 1997; Nakamura & Hanawa 1997; Stehle & Spruit 2001; Li 2001), and follow the 2D cloud evolution in the x - y plane in a Cartesian coordinate system (x, y, z) . Our 2D model is the nonaxisymmetric extension of the 1D model of Li (2001). We assume that the disk is threaded by an ordered magnetic field which is current-free outside the disk and which becomes uniform far from the cloud with a constant strength $B_{z,\infty}$. Twisting of field lines is possible, as a result of, e.g., magnetic braking; it is ignored here since the type of fragmentation that we will discuss is gravitational in origin and does not rely on rotation (see § 3.1). Magnetic braking of the disk and the associated field twisting can be included in our formulation approximately if so desired (Basu & Mouschovias 1994).

The differential equations governing the evolution of a strongly magnetized disk are given in a vertically integrated form. Mass conservation of the disk is expressed by

$$\frac{\partial \Sigma}{\partial t} + \nabla \cdot (\Sigma \mathbf{V}) = 0, \quad (1)$$

where Σ , t , $\mathbf{V} = (V_x, V_y)$ are, respectively, the surface density, time, and velocity in the disk. The momentum equation is given by

$$\frac{\partial (\Sigma \mathbf{V})}{\partial t} + \nabla \cdot (\Sigma \mathbf{V} \mathbf{V}) + \nabla P + H \nabla \left(\frac{B_z^2}{4\pi} \right) - \frac{B_z \mathbf{B}}{2\pi} + \Sigma \mathbf{g} = 0, \quad (2)$$

where $\mathbf{B} = (B_x, B_y)$, $\mathbf{g} = (g_x, g_y)$, and P is the vertically integrated pressure. The equation for the evolution of the vertical field component is

$$\frac{\partial B_z}{\partial t} + \nabla \cdot (B_z \mathbf{V}_B) = 0, \quad (3)$$

where $\mathbf{V}_B = (V_{B,x}, V_{B,y})$ is the velocity vector of magnetic field lines in the disk plane.

The governing equations (1)-(3) are supplemented by the vertically integrated equation of state

$$P = c_s^2 \Sigma, \quad (4)$$

where c_s is the (effective) isothermal sound speed, which we take to be a constant since we are interested in fragmentation during the isothermal regime; the transition to optically thick, adiabatic regime of cloud evolution will be treated elsewhere. We do not consider explicitly in the equation of state the presence and possible decay of turbulence, although some of its effects can be incorporated into the effective sound speed c_s (Lizano & Shu 1989). The ‘‘turbulent’’ pressure should have little direct effect on the

process of fragmentation, which occurs at relatively high densities where the turbulent motions are observed to be subsonic (Myers 1999). It does have a great influence on the initial conditions for our cloud evolution, given in the present study by prescription (see § 2.2).

In addition, we can relate the disk half-thickness to the mass density ρ through

$$H = \Sigma / (2\rho). \quad (5)$$

Assuming hydrostatic equilibrium in the vertical direction of the disk, we find

$$\rho = \frac{\pi G \Sigma^2}{2c_s^2} \left(1 + \frac{B_x^2 + B_y^2}{4\pi^2 G \Sigma^2} \right) + \frac{P_e}{c_s^2}, \quad (6)$$

to the lowest order in (H/r) , where the cylindrical radius $r = (x^2 + y^2)^{1/2}$. The two terms in the brackets represent, respectively, the gravitational compression and magnetic squeezing of the disk material. The quantity P_e is the ambient pressure that helps confine the disk, especially in low column density regions where gravitational compression is relatively weak.

In a lightly ionized medium such as molecular cloud, the field lines slip relative to the neutral matter at a velocity

$$\mathbf{V}_B - \mathbf{V} = \frac{t_c}{\Sigma} \left[\frac{B_z \mathbf{B}}{2\pi} - H \nabla \left(\frac{B_z^2}{4\pi} \right) \right], \quad (7)$$

where the coupling time between the magnetic field and neutral matter, t_c , is given approximately by

$$t_c = \frac{1.4}{\gamma C \rho^{1/2}}, \quad (8)$$

in the simplest case where the coupling is provided by ions that are well tied to the field lines and the ion density ρ_i is related to the cloud density ρ by the canonical expression $\rho_i = C\rho^{1/2}$. Here, $\gamma C = 1.05 \times 10^{-2} \text{ cm}^{3/2} \text{ g}^{-1/2} \text{ s}^{-1}$ (Shu 1991) and the factor 1.4 comes from the fact that the cross section for ion-helium collision is small compared to that of ion-hydrogen collision (Mouschovias & Morton 1991). More detailed treatments of the magnetic coupling including the effects of dust grains are possible (e.g., Nishi, Nakano & Umebayashi 1991). We postpone such treatments to a future study.

The gravitational acceleration \mathbf{g} and field strength \mathbf{B} in the disk plane are determined from the gravitational potential $\psi_G(x, y, z)$ and magnetic potential $\psi_B(x, y, z)$, which satisfy

$$\nabla^2 \psi_G = 4\pi G \Sigma \delta(z), \quad (9)$$

and

$$\nabla^2 \psi_B = (B_z - B_{z,\infty}) \delta(z), \quad (10)$$

where δ is the Dirac delta function.

2.2. Initial Conditions

The initial conditions for the core formation are not well determined either observationally or theoretically. Following Basu & Mouschovias (1994) and Li (2001), we prescribe a reference state in which the clouds are axisymmetric, slowly rotating, and are threaded by a uniform magnetic field, $B_{z,\text{ref}}(x, y) = B_{z,\infty}$. The reference surface density and rotation velocity distributions are taken, respectively, to have the form

$$\Sigma_{\text{ref}}(x, y) = \frac{\Sigma_{0,\text{ref}}}{[1 + (r/r_0)^n]^{4/n}}, \quad (11)$$

and

$$V_{\phi,\text{ref}}(x, y) = \frac{4 \omega r}{r_0 + \sqrt{r_0^2 + r^2}} c_{s,\text{eff}}, \quad (12)$$

where the exponent n controls the surface density profile and (indirectly) the amount of mass in the central plateau region where the distribution is more or less uniform, and the dimensionless parameter ω measures the rotation rate relative to $c_{s,\text{eff}} = c_s(1 + \Gamma_0^2)^{1/2}$, which is essentially the magnetosonic speed (the magnetic contribution comes in through the parameter Γ_0 to be defined in the next paragraph). The somewhat arbitrary profile (11) is chosen mainly to minimize numerical edge effects; it should not be confused with the plateau-plus-envelope density distribution observed in several starless dense cores (Ward-Thompson et al. 1999; Shirley et al. 2000) and used as the initial conditions for some cloud collapse calculations (e.g., Boss 2002)—the observed profile develops naturally in the central part of our model cloud later on through ambipolar diffusion-driven evolution. Note that the rotational velocity prescribed by equation (12) increases linearly with radius inside r_0 before asymptoting to a constant value at larger radii.

The background field strength is characterized by the dimensionless flux-to-mass ratio $\Gamma_0 = B_{z,\infty} / (2\pi G^{1/2} \Sigma_{0,\text{ref}})$, which must be greater than unity for the cloud to be magnetically subcritical. The reference clouds are not in an equilibrium state and are allowed to evolve into one with magnetic field frozen-in, before ambipolar diffusion is turned on at time $t = 0$. To save computational time, we obtain the initial, axisymmetric equilibrium state using the 1D code of Li (2001), in which the cloud radius is chosen to be twice the characteristic radius r_0 for numerical convenience. At $t = 0$, we superpose on top of the equilibrium column density $\Sigma_0(x, y)$ a nonaxisymmetric perturbation of fractional amplitude A , so that

$$\Sigma(x, y) = \Sigma_0(x, y) [1 + A \cos(m\phi)], \quad (13)$$

where ϕ is the azimuthal angle measured from the x -axis. Both the $m=2$ bar mode and higher order modes will be considered in the present study, as well as a form of random perturbation (see §3.5). The subsequent, ambipolar diffusion-driven evolution of the perturbed cloud is followed numerically, subject to the condition of fixed external pressure and B_z at the cloud outer boundary.

2.3. Numerical Methods

Our calculations are carried out using an MHD code based on that of Nakamura & Hanawa (1997). The hydrodynamic part is solved using Roe's TVD (Total Variation Diminishing) method given in Hirsch (1990). To achieve the second-order accuracy, we implemented the so-called "MUSCL" (Monotone Upstream-centered Schemes for Conservation Laws) approach, in which the physical quantities between two adjacent cells are extrapolated to the cell boundary and the linearized Riemann problem is solved exactly for the numerical fluxes at the cell boundaries. The minmod limiting function is used to satisfy the TVD condition. The magnetic part is treated as follows. The equation for magnetic field evolution has a form identical to that for mass conservation, and is solved in the

same manner. Both the magnetic and gravitational potentials satisfy the Poisson equation with a source term containing $\delta(z)$, and both of them are solved using a convolution method described in Hockney & Eastwood (1981). The time step is determined by the Courant-Friedrich-Levy (CFL) condition, with a contribution from the magnetic field included (see also Stehle & Spruit 2001). The original code has been tested with many test problems, including 1D shock tube and point explosion. The tests have verified that the code has second-order accuracy and produces no oscillations of numerical origin (e.g., Matsumoto, Hanawa, & Nakamura 1997). In addition, we have followed the evolution of a set of unperturbed axisymmetric clouds with both the 2D code developed here and the 1D code of Li (2001). The cloud evolution time, surface density distribution, magnetic field strength and gravitational acceleration obtained with the two codes all agree to within a few percent.

Following Nakamura et al. (1999), we employ a zooming technique to resolve the dense, small-scale structures that develop during the cloud evolution. We refine and zoom-in the computational grid whenever the so-called Jeans condition is about to be violated (Truelove et al. 1997), taking into account the magnetic effect on Jeans condition. For production runs, we start all simulations on a 256×256 uniform, rectangular grid. The grid points are doubled in each direction at the first refinement, without changing the size of the simulation box. At each subsequent refinement, the computational domain for hydrodynamics is shrunk by half in each direction, leaving the grid number unchanged (512×512). All physical quantities at the domain boundary are fixed during a given level of (subsequent) refinement. In our calculations, this boundary condition is identical to an inflow boundary condition because, when refinements are needed, the cloud mainly collapses toward the central high density region (although some transient outflows are possible). All physical quantities on the refined grids are obtained by linear interpolation. As a convergence test, we have doubled the initial grid number from 256×256 to 512×512 for a “standard” model (see Table 1 and § 3.2) and found no significant differences. In a future study, we plan to take a nested-grid approach, rather than zooming, which should improve the boundary condition.

The actual numerical computations are carried out using non-dimensional quantities. The units we adopted are $c_s = 1.88 \times 10^4 T_{10}^{1/2} \text{ cm s}^{-1}$ for speed (where T_{10} is the effective temperature in units of 10 K), $\Sigma_{0,\text{ref}} = 4.68 \times 10^{-3} A_V \text{ g cm}^{-2}$ for surface density (where A_V is the visual extinction vertically through the disk for standard grain properties), and $B_{z,\infty} = 7.59 A_V \Gamma_0 \mu\text{G}$ for magnetic field strength (where Γ_0 is the flux-to-mass ratio in units of the critical value). The units for length, time, and mass are, respectively, $L_0 \equiv c_s^2 / (2\pi G \Sigma_{0,\text{ref}}) = 5.83 \times 10^{-2} T_{10} / A_V \text{ pc}$, $t_0 \equiv c_s / (2\pi G \Sigma_{0,\text{ref}}) = 3.03 \times 10^5 T_{10}^{1/2} / A_V \text{ yr}$, and $M_0 \equiv \Sigma_{0,\text{ref}} L_0^2 = 7.64 \times 10^{-2} T_{10}^2 / A_V M_\odot$. We normalize the external pressure by $2\pi G \Sigma_{0,\text{ref}}^2$, and set its dimensionless value to 0.025 for all models.

3. NUMERICAL RESULTS

The number of parameters needed to completely specify the model cloud and imposed perturbation is rather large. These include the characteristic radius r_0 , exponent n in the reference surface density distribution, rotation parameter ω , and dimensionless flux-to-mass ratio Γ_0 for the cloud, and the order m and fractional amplitude A for the perturbation. We have carried out a systematic survey of these parameters as well as a form of random perturbation (of mixed modes), and selected the models listed in Table 1 to illustrate the salient features of magnetic cloud fragmentation.

3.1. Cloud Fragmentation Without Rotation

To begin with, we consider a non-rotating ($\omega = 0$) cloud with the reference state specified by a set of parameters $r_0 = 5\pi$, $n = 8$, and $\Gamma_0 = 1.5$. The cloud is therefore magnetically subcritical, with the field strength 50% above the critical value at the center. This set of parameters is chosen because, in the absence of any nonaxisymmetric perturbations, the cloud so specified would collapse to produce a dense supercritical ring, which is prone to fragmentation. The reference cloud is allowed to evolve into an equilibrium configuration, with the magnetic field frozen-in. After the equilibrium is reached, we reset the time to $t = 0$, and apply an $m = 4$ perturbation to the surface density distribution, with a fractional amplitude of $A = 0.05$. The evolution of such nonaxisymmetrically perturbed cloud is followed numerically to progressively higher densities and smaller scales. The results are shown in panels (a) through (e) of Fig. 1 and described as follows.

As is usual with ambipolar diffusion-driven evolution, the cloud spends most of its time in the subcritical phase when the dimensionless minimum flux-to-mass ratio (at the density peak) $\Gamma > 1$ (see panels a and b of Fig. 1). During this period, inward and outward motions coexist. Both are very subsonic, and exhibit an overall oscillatory pattern (of small amplitude). The oscillation signifies that the cloud is stable to the added $m = 4$ perturbation during the subcritical phase, in agreement with linear analysis by Nakano (1988) and others. Indeed, we have verified numerically that for a frozen-in field the subcritical cloud remains stable to this and other modes. Once the minimum flux-to-mass ratio has dropped below the critical value, the cloud evolution enters a qualitatively new phase. Its contraction accelerates, with speeds first approaching, and eventually exceeding, the sound speed (see panels c-e). It is during this phase that fragmentation occurs. The beginning stage of the fragmentation is shown in panel c), where the velocity vectors deviate significantly from the radial direction in some regions, creating appreciable distortions in the surface density distribution. By the time shown in panel d), the inflow appears to have converged preferentially toward individual pockets, creating four well-defined blobs or fragments. These blobs grow quickly in (surface) density, and become cleanly separated from the background—a common envelope—and from one another by the end of the computation (panel e), when the peak surface density has increased over its reference value by more than a factor of 600. The high density blobs resemble in every way the single (starless) cores obtained in previous calculations, except of course the presence of

neighbors; they are simply multiple dense cores¹.

The multiple cores shown in panel e) are formed together, at separations nearly two orders of magnitude smaller than the central plateau part of the original cloud, from which the cores are condensed out of. The cores are clearly supercritical, with a minimum flux-to-mass ratio of only $\Gamma = 0.62$. They are collapsing dynamically, and are well on their way to forming individual stars or stellar systems. Note that the cores are significantly elongated, with an aspect ratio of roughly 3. The degree of elongation should increase rapidly before density singularities develop due to Lin-Mestel-Shu (1965) instability, forming highly elongated bars by the time the isothermal approximation starts to break down, as in the collapse of single, isolated cores studied by Nakamura & Li (2002). We expect the bars to break up during the subsequent adiabatic phase of cloud evolution, each forming perhaps a binary or multiple system. Together, we anticipate the production of a small stellar group in the cloud as a likely outcome, although we are unable to follow the evolution further because of the increasing demand on spatial resolution.

The properties of cloud fragmentation depend somewhat on the flux-to-mass ratio of the reference state Γ_0 (> 1). Exact values of Γ_0 are difficult to determine observationally; they probably lie within a factor of two of unity (Crutcher 1999), after correcting for likely projection effects (Shu et al. 1999). Subcritical clouds with higher Γ_0 contract more slowly, allowing more time for nonaxisymmetric perturbations to grow. As a result, fragmentation is achieved more readily, at a lower surface density. This beneficial effect of a stronger magnetic field is illustrated in panel f), which displays the density distribution and velocity field of a cloud with $\Gamma_0 = 2$ (instead of 1.5) and other parameters identical to those of the first model at a time when the maximum surface density $\Sigma_{\max} = 10^2$. Clearly, four well-developed cores have already formed. In contrast, at similar values of Σ_{\max} , the cores in the more weakly magnetized $\Gamma_0 = 1.5$ cloud are either absent (panel c) or barely visible (panel d). Note that the positions of the cores are different by about 45 degrees in the two models. This is because the more strongly magnetized $\Gamma_0 = 2$ cloud spent more time in the quasi-static phase, which enabled an additional half cycle of oscillation.

The cores in both models are distributed around a central region of relatively low surface density and high flux-to-mass ratio, signifying their close connection to the ring formed in the absence of perturbation (Li 2001). We stress that the ring formation and its fragmentation do not rely on rotation, which is essential in some non-magnetic models of cloud fragmentation (e.g. Boss 1996; Klapp & Sigalotti 1998). The inclusion of a small amount of rotation, as inferred from molecular line observations of dense cores (Goodman et al. 1993), enhances the magnetic cloud fragmentation somewhat but does not change its behavior fundamentally, as we demonstrate next.

3.2. Standard Model with Small Rotation

¹ Operationally, we identify any local maximum in surface density enclosed within one or more closed contours as a “core”, even though the core may be highly elongated (and thus more filament-like) and, in the case of modest contrast with background, its existence depends on the number of contour levels chosen.

² The true 3D structure would be triaxial, as inferred observationally for dense cores by Jones, Basu & Dubinski (2001) and Goodwin, Ward-Thompson & Whitworth (2002).

To gauge the effects of a slow rotation, we repeat the evolution of a cloud with all parameters identical to those of the first model in the last subsection except the rotation parameter ω , which is set to 0.1 instead of zero. Snapshots of the surface density distribution and velocity field at six selected times are shown in Fig. 2. The general trend of the cloud evolution is similar to that in the non-rotating case, with the fragmentation proceeding unimpededly only after the minimum flux-to-mass ratio drops below the critical value. As before, four distinct blobs have grown by the end of the computation from the initially imposed $m = 4$ perturbation of the same modest amplitude $A = 0.05$, at separations roughly twice those of the non-rotating case. The most noticeable difference besides the swirling pattern of the velocity field (i.e., rotation) is that the cores separate out from the background at a lower maximum surface density Σ_{\max} (compare Fig. 1d and Fig. 2e), pointing to a beneficial effect of the slow rotation on fragmentation. This effect derives from the fact that rotation retards the radial infall, which allows more time for the perturbations to grow and fragments to separate out from the background. We expect the rotation to play an even greater role on the cloud dynamics as the evolution proceeds to smaller scales. It should be a crucial ingredient in determining the orbits of the stars formed. For these reasons, we shall include a slow rotation of $\omega = 0.1$ in all of the models to be discussed hereafter. This model (especially panel e where $\Sigma_{\max} = 10^2$), with a set of “standard” parameters— $r_0 = 5\pi$, $n = 8$, $\omega = 0.1$, $\Gamma_0 = 1.5$, $A = 0.05$ and $m = 4$ —serves as a benchmark against which other models will be compared.

3.3. Different Modes of Perturbation

Four dense cores are formed in the standard model with an $m = 4$ mode of perturbation. It is natural to ask whether other modes of perturbation with different values of m can also induce cloud fragmentation and, if yes, whether the number of cores produced always matches the value of m . To address these issues, we vary the parameter m and keep all other parameters fixed at their value in the standard model. The results at a time when the maximum surface density has increased by two orders of magnitude over its reference value (i.e., $\Sigma_{\max} = 10^2$, as in Fig. 2e for the standard model) are displayed in Fig. 3 for a set of six selected modes with $m = 2, 3, 5, 8, 11$, and 14.

The cloud evolution in the $m = 2$ case resembles those studied previously by Nakamura & Li (2002): soon after the central region becomes supercritical, the perturbation grows nonlinearly into a bar² of aspect ratio of roughly 2. The bar becomes increasingly more elongated as the collapse continues, reaching an aspect ratio of ~ 5 by the time shown in panel a) of Fig. 3. We have followed the cloud evolution further in time, to a central density where the isothermal approximation starts to break down. The bar got more elongated still, but did not break up into pieces. Therefore, unlike the $m = 4$ case, fragmentation into discrete cores does not occur, at least during the isothermal phase of cloud evolution, consistent with previous studies

of the collapse of non-magnetic filaments (e.g., Truelove et al. 1997; Sigalotti & Klapp 2001). In this regard, the $m = 2$ mode is different from the $m = 4$ (and other higher order) mode.

The cloud perturbed with an $m = 3$ mode appears to evolve in a way intermediate between the $m = 2$ and $m = 4$ cases. On the one hand, the perturbation has become highly nonlinear by the time shown in panel b), but no discrete blobs are visible, as in the $m = 2$ case (panel a). On the other hand, if we continue the evolution further, the cloud does eventually break up into (three) discrete cores, as in the benchmark $m = 4$ case (see Fig. 2). We speculate that this intermediate behavior derives from the fact that the $m = 3$ mode distorts more severely than the $m = 4$ mode the ring that would have formed in the absence of any perturbations (perhaps through preferential central density enhancement) but less so than the $m = 2$ mode; the breakup into discrete cores appears to be intimately linked to ring fragmentation.

Five cores are produced in the $m = 5$ case, as shown in panel c). The core appearances are quiet different from one another, much more so than for example those in the $m = 4$ case, even though the initial perturbation is periodic azimuthally. We believe that the symmetry is broken by numerical noises, and amplified by gravity; our rectangular computational grid appears to have affected the odd modes (such as the $m = 5$ mode shown here and the $m = 11$ mode to be discussed below) more than the even modes (such as the benchmark $m = 4$ mode and the $m = 8$ and 14 modes below). Furthermore, the $m = 5$ (and any other) mode is not an eigenmode of the (evolving) cloud. Differential growth of the eigenmodes contained in the initial perturbation may have also contributed to the noted symmetry breaking.

In each of the three cases with higher order modes ($m = 8, 11$ and 14), four blobs are clearly noticeable by the time shown in panels d)-f). The cores (or rather filaments) are highly elongated, with the potential of further breakup at higher densities before the isothermal approximation breaks down. The equal number of fragments in all three cases is interesting, indicating that the fragment number does not necessarily increase with the value of m . It is limited, in our view, by the number of Jeans masses contained in the high-density ring in which the filaments are embedded. Note that the blobs in the $m = 14$ case start to separate out from the background (ring) material at a higher surface density than the other two (lower m) cases, presumably because the (nonradial gravitational) force responsible for ring fragmentation is cancelled out to a larger extent due to more rapid azimuthal variation in the perturbed mass distribution. The number of fragments depends somewhat on the perturbation amplitude. For example, eight (rather than four) discrete cores are produced in the $m = 8$ case at a similar time (when $\Sigma_{\max} = 10^2$) for a larger perturbation of fractional amplitude $A = 0.3$ (instead of 0.05).

To summarize, we find that, for the standard cloud, a bar grows out of the $m = 2$ mode, in agreement with our previous finding, and for higher order modes discrete cores can be produced. For a modest fractional amplitude of $A = 0.05$ the number of cores formed ranges from 3 to 5 by the time of a 10^2 -fold increase in the maximum surface

density. The fragmentation appears to be most effective for an intermediate range of modes. At the low- m end (for $m = 2$ and to a lesser extent $m = 3$), fragmentation appears difficult, possibly because the surface density increases preferentially at the center, which tends to suppress ring formation. Fragmentation at the high- m end is limited, on the other hand, by the (magnetically modified) Jeans length inside the ring. A larger fractional amplitude of the perturbation may change this conclusion quantitatively, but not qualitatively.

We note that the elongated multiple dense cores in the $m \geq 3$ cases (especially those filament-like ones) as well as the bar in the $m = 2$ case will get a second chance at fragmentation after the stiffening of equation of state, producing perhaps an even larger number of discrete fragments that could serve as seeds for star formation.

3.4. Clouds with Different Characteristics

So far, we have concentrated on model clouds whose mass distributions are specified by the pair of parameters $r_0 = 5\pi$ and $n = 8$. We next consider different combinations of r_0 and n . The characteristic radius r_0 is to be compared with 2π , the (dimensionless) critical wavelength for the (thermal) Jeans instability in a disk of uniform mass distribution (Larson 1985). The parameter n controls the profile of the cloud surface density distribution; those with smaller values of n are more centrally peaked.

We first hold the profile parameter fixed at the standard value $n = 8$, and vary the radius r_0 . Representative results are shown in panels a)-d) of Fig. 4, at a time when the maximum surface density $\Sigma_{\max} = 10^2$, as in Fig. 2e and Fig. 3. Panels a) and b) are the snapshots of a cloud with $r_0 = 10\pi$, twice the standard value, perturbed respectively by an $m = 4$ and 8 mode of the standard fractional amplitude $A = 0.05$. In the $m = 4$ case, four dense cores have clearly condensed out of a ring-like structure, similar to those displayed in Fig. 2e for the standard $r_0 = 5\pi$ model. The main difference is that the cores here have achieved a larger density contrast with the background and a higher degree of elongation, indicating that the process of fragmentation has proceeded further at a similar stage of cloud evolution. The core formation is also more dynamic, generating appreciable outward motions which lead to the production (well outside the high-density ring) of several secondary blobs of local density maxima (not shown). These secondary blobs are still magnetically subcritical but appear to be marginally self-gravitating. Whether they will eventually collapse onto themselves and form stars remains uncertain.

In the $m = 8$ case (panel b), four discrete over-dense filaments are embedded in a ring-like structure, similar to the standard $r_0 = 5\pi$ case (see Fig. 3d). Unlike those in Fig. 3d, however, the filaments contain two distinct density peaks (or cores) each, signaling again that the fragmentation has progressed further. Note that one core in each filament is much more prominent than the other, even though the initial perturbation that seeds the core formation is periodic azimuthally. As mentioned earlier, the asymmetry is probably introduced by numerical noises but amplified by gravity, especially after the formation of supercritical cores, the densest of which collapse in a runaway fashion. In any case, these two examples illustrate

that the $r_0 = 10\pi$ cloud is more susceptible to fragmentation than the $r_0 = 5\pi$ cloud. This result is perhaps to be expected, since a larger characteristic radius r_0 implies a larger number of Jeans masses, which is known to enhance the fragmentation of non-magnetic clouds. Our calculations demonstrate that the same trend holds for strongly magnetized clouds as well.

Reducing the radius r_0 is expected to have a negative effect on cloud fragmentation. This is indeed the case, as illustrated in the next two panels of Fig. 4, where $r_0 = 2.5\pi$, half of the standard value. Panel c) shows that the $m = 4$ mode does not grow enough by the time $\Sigma_{\max} = 10^2$ that there is no discernible sign of fragmentation. The surface density peaks at the cloud center, forming a single dense core, just as in the case of no perturbation for this (initially axisymmetric) cloud. We have followed the evolution of the cloud perturbed by other modes, and found rapid growth only for $m = 2$. A snapshot of the $m = 2$ case is shown in panel d), where the presence of a (twisted) bar is evident. It therefore appears that the conditions for the $m = 2$ mode to grow nonlinearly (into bars) are less stringent than those for the higher order modes to cause cloud fragmentation. Note that the bar in panel d) is less elongated than that of the standard $r_0 = 5\pi$ cloud (Fig. 3a), indicating that a reduction in r_0 has hampered not only the cloud breakup (for $m \geq 3$) but also bar growth (for $m = 2$).

We next consider the influence of the initial surface density profile, as specified by the parameter n , on cloud fragmentation. For non-magnetic clouds, it is well established that those with more peaked density profiles are less prone to fragmentation (Boss 1993). We find the same trend for strongly magnetized clouds as well. This is illustrated in the last two panels of Fig. 4, where $n = 2$ (much smaller than the standard value of 8) is chosen, along with the standard radius $r_0 = 5\pi$. In the absence of any nonaxisymmetric perturbation, the cloud collapses into a single central core rather than an off-centered ring, as a result of the reduction in n , which decreases the number of Jeans masses contained in the central plateau region. We find modes with $m \geq 3$ do not grow significantly to induce the cloud to break up into discrete cores, as exemplified by panel e), where the $m = 4$ case is displayed. The $m = 2$ mode does grow nonlinearly into a bar (panel f), although the bar is much less elongated than that in the standard $n = 8$ cloud (Fig. 3a), whose density profile is much flatter in the central region.

To summarize, we find that, as in the non-magnetic case, the ability of a strongly magnetized cloud to fragment into pieces is controlled mainly by the number of Jeans masses contained in the central plateau region. Ring formation under axisymmetry provides a good indicator of whether a cloud breaks up into fragments or not when perturbed nonaxisymmetrically with $m > 2$ modes, but not of bar formation from an $m = 2$ mode. The conditions for bar formation appear to be less stringent than those for cloud fragmentation. If the characteristic radius r_0 and/or profile parameter n are small enough so that the central region becomes more or less thermally dominated³, even bar formation will be inhibited (e.g., $r_0 = 2\pi$ and $n = 2$), let alone fragmentation.

3.5. Random Perturbations and Mode Coupling

Perturbations in star-forming molecular clouds are not expected to be as regular as the single modes treated so far, although their exact nature is still unknown. In this subsection, we will consider the opposite extreme, in which the fractional amplitude of the density perturbation at each grid point is drawn randomly between $-A$ and A . Such random perturbations contain a mixture of modes. The number of fragments produced should reflect to some extent the fastest growing mode and provide another measure of the ability of a cloud to fragment.

We begin with a “canonical” model in which an $r_0 = 7\pi$ cloud is randomly perturbed with a fractional amplitude $A = 0.1$. Other parameters have their standard values (see Table 1). The cloud evolution is shown in the first three panels of Fig. 5, starting with the equilibrium state (panel a), where the perturbation is barely visible. By the time when the maximum surface density has increased by an order of magnitude over its reference value ($\Sigma_{\max} = 10$), three condensations of relatively low contrast in surface density have formed (panel b). They subsequently fragment into five discrete cores, two of which appear to collapse in a runaway fashion (panel c). Again, the cores are significantly elongated, although not as much as those grown out of single-mode perturbations in general, probably as a result of the reduction in the degree of symmetry. In this particular model, the $m = 5$ mode appears to be the fastest growing one among the modes present in the initial random perturbation.

We have followed the evolution of randomly perturbed clouds with different characteristic radius r_0 , and found different numbers of fragments. The results are illustrated in the next two panels of Fig. 5, where $r_0 = 10\pi$ and 5π are adopted, with everything else fixed as in the canonical model, including identical random perturbation at each grid point. Panel d) shows that by the time $\Sigma_{\max} = 10^2$ the same five cores in the canonical $r_0 = 7\pi$ model are also present in the larger/more massive $r_0 = 10\pi$ cloud, with similar relative positions. The relative surface densities are different, however, with the core at the bottom being the densest (rather than the rightmost one). In addition, one core and two condensations of lower density contrast (and a low-density “bubble”) are present, reinforcing the finding that magnetic clouds with more Jeans masses tend to fragment into a larger number of pieces. The smaller/less massive $r_0 = 5\pi$ cloud fragmented into three cores (panel e), pointing to the $m = 3$ mode as the fastest growing one. The result is somewhat surprising, however, since the pure $m = 3$ mode did not produce any discrete cores by the time $\Sigma_{\max} = 10^2$ for this cloud (see Fig. 3b), whereas other modes such as $m = 4$ (Fig. 2e) and 5 (Fig. 3c) did. We suspect that nonlinear mode coupling is involved in the formation of these cores, perhaps by slowing down the growth of the central surface density that may otherwise impede fragmentation.

To demonstrate mode coupling more clearly, we have repeated the canonical model with an additional $m = 2$ mode of a small fractional amplitude $A = 0.01$ superposed. The result is somewhat surprising: by the time $\Sigma_{\max} = 10^2$ (shown in the last panel of Fig. 5), a double-

³ In this limit, the thin-disk approximation adopted in the paper may break down.

core has formed, which differs drastically from both the five cores formed in the canonical model (panel c) and the smooth bar that would grow out of the $m = 2$ mode in the absence of the random perturbation. It appears that, as in the $r_0 = 5\pi$ case shown in panel e), the random perturbation has suppressed the density growth near the center, enabling matter to accumulate preferentially in two cores rather than a continuous bar. The denser of the cores should collapse first into a stellar object (or system). This should not, however, disrupt the less dense core, since it takes much less time for the core material to collapse onto itself than falling toward the other center of gravity. As a result, we anticipate that a wide binary or hierarchic multiple system (if further fragmentation occurs) would be produced, even though the double-core formation is not driven by rotation. Higher resolution calculations, perhaps using moving sink-cell technique, are needed to ascertain the final outcome. We will pursue this intriguing mechanism of (wide) binary formation further elsewhere.

To summarize, we have demonstrated that magnetically supported clouds of masses well above the Jeans limit can fragment into discrete dense cores as a result of ambipolar diffusion, for both single modes and random perturbations. The multiple cores are produced more or less *together* (as opposed to in isolation), both in space and in time. Spatially, they are all located in the magnetically supercritical region, which is much more compact than the original cloud. Temporally, they are produced during the supercritical phase of cloud evolution, which is much shorter than the “coreless” subcritical phase. We have shown that more massive magnetic clouds tend to fragment into a larger number of pieces, as in the nonmagnetic case. These general features are expected to persist for more realistic perturbations, which we plan to explore in the future, perhaps with input from the simulations of turbulent molecular clouds (e.g., Ostriker, Gammie & Stone 1999).

4. DISCUSSION AND CONCLUSION

4.1. Nature of Magnetic Cloud Fragmentation

The beneficial roles of strong, ordered magnetic fields in resolving the thorny “angular momentum problem” of star formation and in preventing the overall dynamical collapse of molecular clouds are well known (Shu et al. 1987; Mouschovias & Ciolek 1999). Their effects on cloud fragmentation are less explored, and appear more subtle. On the one hand, the magnetic pressure can assist the thermal pressure in erasing density inhomogeneities and thus impede fragmentation. On the other hand, the magnetic tension force dilutes gravity, allowing more time for perturbations to grow and over-dense fragments to separate out (see also Boss 2002). The deleterious effects are brought out clearly in the simulations of Phillips (1986a), where the (frozen-in) magnetic fields are taken to be uniform initially, with zero tension force. Phillips (1986a) followed the collapse of a set of such uniformly magnetized clouds with a range in the ratio of thermal to gravitational energies and degree of magnetization. He found that none of the clouds fragmented, even in the presence of a large, 50% density perturbation. We believe that the lack of fragmentation is mainly due to the weakness of the magnetic tension force relative to gravity in his models, which

does not slow down the nearly free-fall collapse appreciably. The tension force is stronger in the models of Phillips (1986b) where the initial fields are non-uniform. However, nonaxisymmetric perturbations are not imposed on these clouds, and it is not clear whether fragmentation is enhanced by the stronger tension force or not. The beneficial effects of magnetic tension force on fragmentation is illustrated most cleanly with the thin-sheet model of Shu & Li (1997), which is threaded everywhere by a (frozen-in) magnetic field of critical strength. In such an idealized cloud, the gravity is exactly balanced by the tension force for arbitrary mass distributions, including those with large numbers of condensations (see Allen & Shu 2000 for a toy model of the fragmentation of critically magnetized clouds induced by protostellar winds).

The opposing effects of magnetic fields on cloud fragmentation call for a numerical attack, especially in the presence of ambipolar diffusion, which changes the relative importance of the two with time. Our calculations demonstrate that, despite these extra complications, the ambipolar diffusion-driven fragmentation of magnetically subcritical clouds has much in common with that of nonmagnetic clouds (e.g., Boss 1996; Klapp & Sigalotti 1998): those clouds containing more Jeans masses and having flatter mass distributions are more susceptible to fragmentation. These trends can be understood qualitatively from the classical Jeans analysis (e.g., Larson 1985) and its extension to lightly ionized, strongly magnetized media (Langer 1978). In both cases, cloud fragmentation involves multiple Jeans masses and is driven by the (magnetically diluted) gravity over the resistance of the (magnetically enhanced) pressure gradient. A major advantage of magnetic clouds over their non-magnetic counterparts is their ability to contain multiple Jeans masses without collapsing promptly. Equally important to fragmentation is the flattening of mass distribution along field lines, which enables self-gravitating off-center pockets to preferentially collapse onto themselves rather than falling toward the center (Larson 1985).

Once the central region of a magnetically supported, multi-Jeans mass cloud has become supercritical, nonaxisymmetric perturbations start to grow. The time for growth is lengthened considerably by the magnetic tension force, which remains strong enough during the initial period of the supercritical phase to balance out the gravity to a large extent. Nakamura & Li (2002) demonstrated that $m=2$ density perturbations of modest fractional amplitude of 5% can grow nonlinearly into bars of aspect ratio ~ 2 during this period (see § 3 for more examples). It is also during this period that cloud breakup into multiple cores occurs, as speculated by Li (2001) and shown explicitly in the paper. This critical phase of cloud evolution enables the (initially) magnetically subcritical clouds to either break up directly into pieces and/or become significantly elongated, setting the stage for possible (further) fragmentation at later times. It is absent from the evolution of both the non-magnetic and (strongly) magnetically supercritical clouds. The beneficial effects of a strong magnetic field on fragmentation are illustrated vividly in Fig. 1, which shows that increasing the field strength of a subcritical cloud makes it easier for the cloud to break up into multiple cores.

Fragmentation of strongly magnetized cloud cores has been examined by Boss in a series of papers (see Boss 2002 for the latest). Using a 3D code that treats the magnetic forces and ambipolar diffusion approximately, he finds that prolate magnetic cores tend to produce binaries and oblate cores multiple systems. Our calculations are similar to his oblate core calculations but with a different focus: the formation of multiple dense cores out of a flattened, more diffuse background cloud⁴. We concur with Boss’s general conclusion that fragmentation can take place *despite* the presence of significant magnetic fields. Indeed, one may go one step further, and speculate that the fragmentation of relatively quiescent clouds into binaries, multiple systems and small groups occurs largely *because* of the strong magnetic field, although more detailed calculations are needed to back up this viewpoint.

4.2. Implications on Small Stellar Group Formation

Magnetically supported clouds can have masses well above the Jeans limit and a naturally-flattened mass distribution, both of which are conducive to the growth of nonaxisymmetric perturbations as the magnetic support weakens with time due to ambipolar diffusion. Nonlinear growth of perturbations produces two basic types of overdense structure in the supercritical phase of cloud evolution: single, isolated bars for the $m = 2$ mode and, for higher order modes, discrete multiple cores, each of which is also significantly elongated in general. Nakamura & Li (2002) have speculated that the elongated dense cores (or bars), with their elongation strongly amplified at higher densities by the Lin-Mestel-Shu (1965) instability, may fragment during the subsequent adiabatic phase of cloud evolution, individually producing perhaps a binary or multiple stellar system. More detailed calculations are needed to put the speculation on a firmer ground. Here, we wish to concentrate on the implications of the multiple cores, whose collapse to form collectively a small group of stars appears more certain. This is because by the end of the computations (some of) the cores have cleanly separated out from the background and from one another, and are well on their way to produce stellar density objects.

Some of the salient features of multiple core formation can be seen from Fig. 2, where the evolution and fragmentation of the benchmark cloud with a slow rotation are displayed. Adopting a fiducial temperature of 10 K and visual extinction of $A_V = 1$, we find that the cloud initially contains a central region of flat surface density distribution of radius ~ 1 pc and mass $\sim 50 M_\odot$. It takes about 5.2 Myrs for the cloud to reach the supercritical state, and another 2.4 Myrs for the $m=4$ perturbations to grow into well-defined multiple dense cores. The cores are separated by ~ 0.05 pc and, at the end of the calculation, have peak extinction of over 300. They are embedded within a much larger common envelope of lower visual extinction. The cores are well on their way to dynamic collapse from inside-out, each expected to form a protostar or protostellar system which grows by accreting mass competitively

from the envelope. In this particular example, we anticipate the formation of a group of stars within a relatively small region of 0.05 pc or less, although detailed properties of the group, such as the final masses of individual members and their orbital elements, are unknown. Our calculation sets the stage for future higher resolution calculations capable of following the subsequent core evolution to the formation of point mass (protostar) and beyond, which would help elucidate such important topics as competitive mass accretion and orbital evolution of the (still accreting) protostars (Bonnell et al. 1997). Substantial orbital evolution is expected of the group members, not only because the dense cores—the raw materials out of which they are formed—are not rotationally supported (from collapsing into one another), but also because the stars can interact gravitationally with the envelope (by raising tides) and with one another. The former tends to shrink the stellar orbits, and the latter may lead to the ejection of some (lighter) members while leaving others more tightly bound. The decay of small-number groups may be an important channel for producing binaries and multiple systems (e.g., Sterzik & Durisen 1999) and, in the scenario of Reipurth & Clarke (2001), be responsible for brown dwarf formation.

How are the magnetically subcritical clouds (or “clumps” following the notations of Williams et al. 2000) of multiple Jeans masses capable of fragmentation created in the first place? We do not have a definitive answer, but suspect that it probably involves in one way or another turbulence, which is strong in the low density regions out of which the subcritical clouds or clumps are condensed. The condensation could occur for example through compression in the converging regions of a turbulent flow (e.g., Ostriker et al. 1999), and/or as a result of localized turbulence decay (Myers 1999). Since the turbulence is highly supersonic, the thermal pressure (and thus the Jeans limit) should have little relevance to the process. One therefore expects clouds or clumps of more than one Jeans mass to be a common product, at least for those more massive, self-gravitating ones that are the sites of star formation. Whether such clouds or clumps are magnetized strongly enough to be subcritical or not is unclear. As yet, there is not enough direct Zeeman measurements of field strength in relatively low density regions to provide a firm answer to this crucial question one way or the other (Crutcher 1999). In the the standard scenario of isolated low-mass star formation the clumps are envisioned to be magnetically subcritical (Shu et al. 1987; Mouschovias & Ciolek 1999). If this turns out to be the case, then their propensity for containing more than one Jeans mass would make them suitable for group formation.

There is some observational evidence that small groups are a common product of low-mass star formation, in both the so-called “isolated” and “clustered” modes (Shu et al. 1987). The archetype of the former is the Taurus molecular cloud. Molecular line surveys of this nearby dark cloud in ^{13}CO (Mizuno et al. 1995; at a spatial resolution of ~ 0.1 pc), C^{18}O (Onishi et al. 1996; ~ 0.1 pc) and H^{13}CO^+

⁴ Even though our discussions of the dimensionless solutions of cloud evolution are centered on relatively low initial densities appropriate for pre-core conditions, it may be possible to reinterpret these solutions using (oblate) dense cores as the starting point (if such cores are magnetically subcritical). In this reinterpretation, the discrete overdense blobs developed toward the end of our calculations would have much higher densities and smaller separations, comparable to the multiple protostellar fragments found by Boss (2002). The fact that these two very different sets of calculations (different geometries, numerical methods and treatments of radiative transfer, magnetic field and ambipolar diffusion) yield qualitatively similar results regarding fragmentation is reassuring.

(Onishi et al. 1999; ~ 0.01 pc) have found an apparent threshold in the H_2 surface density of $\sim 8 \times 10^{21} \text{ cm}^{-2}$ for ongoing star formation, as marked by either dense compact (pre-stellar) $H^{13}CO^+$ cores or “cold” (in IR colors) young stellar objects (YSOs; Onishi et al. 1998). Interestingly, those star-forming $C^{18}O$ cores above the threshold typically contain more than one compact core and/or cold YSO, with the more massive ones associated with a larger number of cold objects. Higher resolution continuum maps have also revealed many examples of dust condensations in close proximity, with separations of order ~ 0.1 pc or less (e.g., Looney, Mundy & Welch 2000; Shirley et al. 2000; Motte & Andre 2001). These groupings of pre-stellar objects and YSOs in relatively quiescent regions could result from the ambipolar diffusion-driven fragmentation of magnetically supported clouds discussed in this paper. Even more striking examples of such groupings can be found in cluster-forming regions, such as the fragmented ring-like structure in the Serpens cloud core (Williams & Myers 2000) and the dozen or so starless fragments in the ρ Oph B2 core (Motte et al. 1998). Whether they could be produced in the same manner is less certain, complicated by the strong turbulence, which is present in these regions but not treated explicitly in our calculations.

One prediction of our scenario is that the group members would have rather small spread in age even though they are formed through ambipolar diffusion, a process that can take up to 10 Myrs. The reason is that the dense cores are produced in our picture together during the supercritical phase, which lasts for a small fraction of the total time of cloud evolution. Even though the denser of the cores would collapse to form stars first, the spread in stellar age should still be relatively small, perhaps comparable to that of stars formed from the fragmentation of non-magnetic clouds—much less than the spread of those

formed from separate subcritical clouds in complete isolation from one another.

4.3. Conclusion and Future Work

To summarize, we have followed numerically the ambipolar diffusion-driven evolution of magnetically supported molecular clouds in the presence of various non-axisymmetric modes of perturbations. We confirmed our previous finding that the $m = 2$ perturbations of modest amplitude grow readily into bars, which have implications for binary and multiple system formation. Clouds perturbed with higher order modes can break up into multiple cores, which should collapse to form collectively small groups of stars. These calculations are the first step toward a comprehensive theory of multiple star formation in strongly magnetized clouds.

Our calculations are limited to the isothermal regime. They will be extended into the adiabatic regime at higher densities, to follow the expected breakup of the (long) bars and multiple cores, which are also significantly elongated in general. A new feature at the higher densities is the magnetic decoupling (e.g., Nishi et al. 1991), which will require a more elaborate treatment of the magnetic coupling than the one we adopted. Ultimately, we would like to continue our calculations into the protostellar accretion phase, hoping to determine the masses of individual stars and their orbits, perhaps with an approximate treatment of the magnetic braking which may significantly affect the angular momentum evolution of the system.

Numerical computations in this work were carried out at the Yukawa Institute Computer Facilities, Kyoto University. F.N. gratefully acknowledges the support of the JSPS Postdoctoral Fellowships for Research Abroad. We thank the referee for a prompt and helpful report.

REFERENCES

- Allen, A. & Shu, F. H. 2000, *ApJ*, 536, 368
 Basu, S. & Mouschovias, T. 1994, *ApJ*, 432, 720
 Bodenheimer, P., Burkert, A., Klein, R. I., & Boss, A. P. 2000, in *Protostars and Planets IV*, ed. V. Mannings, A. P. Boss, & S. S. Russell (Tucson:University of Arizona Press), p. 675
 Bonnell, I. A., Bate, M. R., Clarke, C. J. & Pringle, J. E. 1997, *MNRAS*, 285, 201
 Boss, A. P. 1993, *ApJ*, 410, 157
 —, 1996, *ApJ*, 468, 784
 —, 2002, *ApJ*, 568, 743
 Caselli, P., Walmsley, C. M., Zucconi, A., Dore, L. & Myers, P. C. 2002, *ApJ*, 565, 344
 Ciolek, G. E. & Basu, S. 2000, *ApJ*, 529, 925
 Ciolek, G. E. & Mouschovias, T. 1993, *ApJ*, 418, 774
 Crutcher, R. M. 1999, *ApJ*, 520, 706
 Crutcher, R. M., Mouschovias, T., Troland, T. H. & Ciolek, G. E. 1994, *ApJ*, 427, 839
 Crutcher, R. M. & Troland, T. H. 2000, *ApJ*, 537, L139
 Dorfi, E. 1982, *A&A*, 114, 151
 Fiedler, R. & Mouschovias, T. 1993, *ApJ*, 415, 680
 Galli, D., Shu, F. H., Laughlin, G., & Lizano, S. 2001, *ApJ*, 551, 367
 Goodman, A., Benson, P., Fuller, G., & Myers, P. 1993, *ApJ*, 406, 528
 Goodwin, S. P., Ward-Thompson, D. & Whitworth, A. P. 2002, *MNRAS*, 333, 769
 Hirsch, C. 1990, *Numerical Computation of Internal and External Flows Volume 2: Computational Methods for Inviscid and Viscous Flows* (John Wiley & Sons), Chapters 20 and 21
 Hockney, R. W. & Eastwood, J. W. 1981, *Computer Simulation using Particles* (New York: McGraw Hill), p. 211
 Indebetouw, R. & Zweibel, E. G. *ApJ*, 2000, 532, 361
 Jones, C. E., Basu, S., & Dubinski, J. 2001, *ApJ*, 551, 387
 Klapp, J. & Sigalotti, L. 1998, *ApJ*, 504, 158
 Langer, W.D. 1978, *ApJ*, 225, 95
 Larson, R. B. 1985, *MNRAS*, 214, 379
 Li, Z.-Y. 2001, *ApJ*, 526, 806
 Li, Z.-Y., Schematovich, V., Wiebe, D. & Shustov, B. 2002, *ApJ*, 569, 792
 Lin, C. C., Mestel, L., & Shu, F. H. 1965, *ApJ*, 142, 1431
 Lizano, S. & Shu, F. H. 1989, *ApJ*, 342, 834
 Looney, L. W., Mundy, L. G. & Welch, W. J. 2000, *ApJ*, 529, 477
 Matsumoto, T., Hanawa, T., & Nakamura, F. 1997, *ApJ*, 478, 569
 Mizuno, A., Onishi, T., Yonekura, Y., et al. 1995, *ApJ*, 445, L161
 Motte, F. & Andre, P. 2001, *A&A*, 365, 440
 Motte, F., Andre, P. & Neri, R. 1998, *A&A*, 336, 150
 Mouschovias, T. & Morton, S. A. 1991, *ApJ*, 371, 296
 Mouschovias, T. & Ciolek, G. 1999, in *The Origins of Stars and Planetary Systems*, ed. C. Lada & N. Kylafis (Kluwer), p. 305
 Myers, P. C. 1999, in *The Origins of Stars and Planetary Systems*, ed. C. Lada & N. Kylafis (Dordrecht: Kluwer), p. 67
 Nakamura, F. & Hanawa, T. 1997, *ApJ*, 480, 701
 Nakamura, F., Hanawa, T., & Nakano, T. 1995, *ApJ*, 444, 770
 Nakamura, F. & Li, Z.-Y. 2002, *ApJ*, 566, L101
 Nakamura, F., Matsumoto, T., Hanawa, T., & Tomisaka, K. 1999, *ApJ*, 510, 274
 Nakano, T. 1979, *PASJ*, 31, 697
 —, 1988, *PASJ*, 40, 593
 —, 1998, *ApJ*, 494, 587
 Nishi, R., Nakano, T., & Umebayashi, T. 1991, *ApJ*, 368, 181
 Onishi, T., Mizuno, A., Kawamura, A., et al. 1996, *ApJ*, 465, 815
 —, 1998, *ApJ*, 502, 296
 Onishi, T., Mizuno, A., Kawamura, A., & Fuhui, Y. 1999, in *Star Formation 1999*, ed. T. Nakamoto (Nobeyama Radio Observatory), p. 153
 Ostriker, E. C., Gammie, C. F. & Stone, J. M. 1999, *ApJ*, 513, 259
 Phillips, G. J. 1986a, *MNRAS*, 221, 571

- , 1986b, MNRAS, 222, 111
 Reipurth, B. & Clarke, C. 2001, ApJ, 122, 432
 Shirley, Y. L., Evans, N. J., Rawlings, J. & Gregersen, E. M. 2000, ApJS, 131, 249
 Shu, F. H. 1991, The Physics of Astrophysics II (Mill Valley: University Science Books)
 Shu, F. H., Adams, F. C., & Lizano, S. 1997, ARA&A, 25, 23
 Shu, F. H., Allen, A., Shang, H., Ostriker, E., & Li, Z.-Y. 1999, in The Origins of Stars and Planetary Systems, ed. C. Lada & N. Kylafis (Kluwer) p. 540
 Shu, F. H. & Li, Z.-Y. 1997, ApJ, 475, 251
 Sigalotti, L. Di G. & Klapp, J. 2001 A&A, 378, 165
 Stehle, R. & Spruit, H. C. 2001, MNRAS, 323, 587
 Sterzik, M. F. & Durisen, R. H. 1999, in Star Formation 1999, ed. T. Nakamoto (Nobeyama Radio Observatory), p. 387
 Tafalla, M., Mardones, D., Myers, P. C., et al. 1998, ApJ, 504, 900
 Truelove, J. K., Klein, R. I., McKee, C. F., Holloman II, J. H., Howell, L. H., & Greenough, J. A. 1997, ApJ, 489, L179
 Ward-Thompson, D., Motte, F. & André, P. 1999, MNRAS, 305, 143
 Williams, J. P., Blitz, L. & McKee, C. F. 2000, in Protostars and Planets IV, ed. V. Mannings, A. P. Boss, & S. S. Russell (Tucson:University of Arizona Press), p. 97
 Williams, J. P. & Myers, P. C. 2000, ApJ, 537, 891

TABLE 1
PARAMETERS OF MODELS

| r_0 | n | ω | Γ_0 | perturbation | A | display |
|----------|-----|----------|------------|--------------------------|--------------|------------------|
| 5π | 8 | 0.0 | 1.5 | $m = 4$ | 0.05 | Fig.1a-e |
| 5π | 8 | 0.0 | 2.0 | $m = 4$ | 0.05 | Fig.1f |
| 5π | 8 | 0.1 | 1.5 | $m = 4$ | 0.05 | Fig.2a-f * |
| 5π | 8 | 0.1 | 1.5 | $m = 2, 3, 5, 8, 11, 14$ | 0.05 | Fig.3a,b,c,d,e,f |
| 10π | 8 | 0.1 | 1.5 | $m = 4, 8$ | 0.05 | Fig.4a,b |
| 2.5π | 8 | 0.1 | 1.5 | $m = 4, 2$ | 0.05 | Fig.4c,d |
| 5π | 2 | 0.1 | 1.5 | $m = 4, 2$ | 0.05 | Fig.4e,f |
| 7π | 8 | 0.1 | 1.5 | random | 0.1 | Fig.5a-c ** |
| 10π | 8 | 0.1 | 1.5 | random | 0.1 | Fig.5d |
| 5π | 8 | 0.1 | 1.5 | random | 0.1 | Fig.5e |
| 7π | 8 | 0.1 | 1.5 | random and $m = 2$ | 0.1 and 0.01 | Fig.5f |

Note. — All models are computed on an initial grid of 256×256 in the disk (x - y) plane. The grid number is increased to 512×512 for each level of refinement. The third model from the top (marked by *) is the “standard” model against which others are compared, and the “canonical” randomly-perturbed model is marked by **.

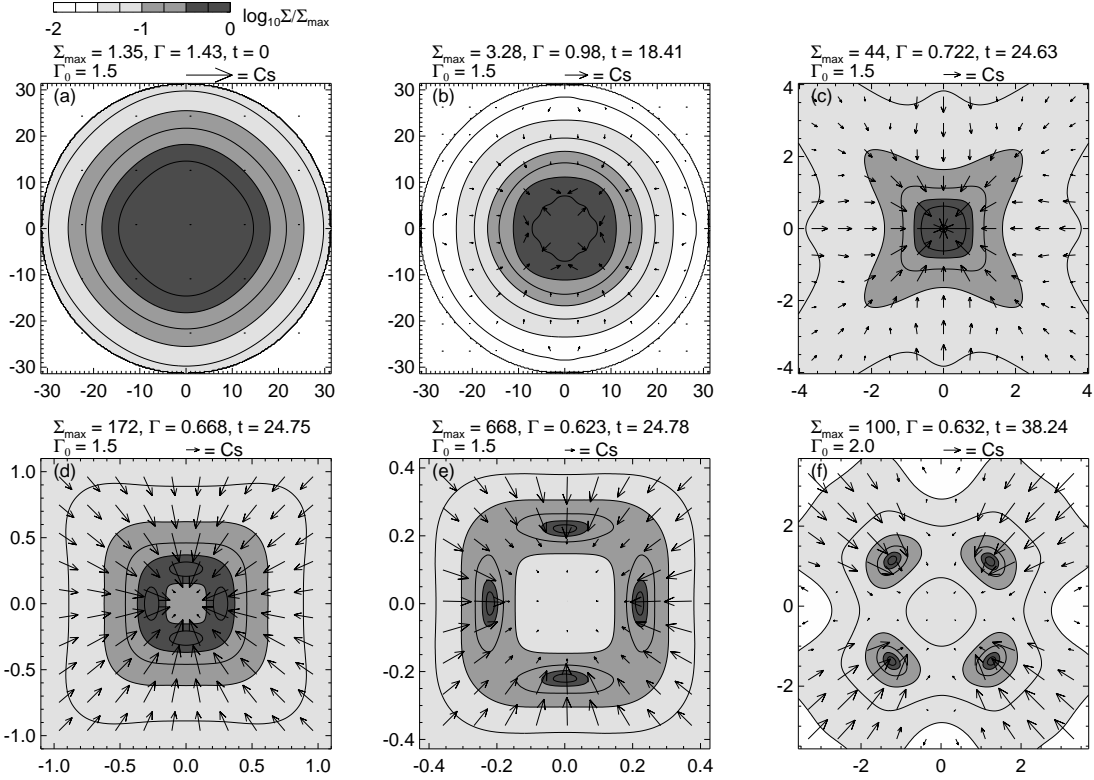


FIG. 1.— Snapshots of the surface density distribution and velocity field for two strongly magnetized, non-rotating clouds perturbed by an $m = 4$ mode of fractional amplitude $A = 0.05$. Panels (a) through (e) show the evolution and fragmentation of a cloud specified by parameters $(r_0, n, \omega, \Gamma_0) = (5\pi, 8, 0, 1.5)$, and panel (f) illustrates the beneficial effect of a stronger magnetic field (with $\Gamma_0 = 2.0$ rather than 1.5) on fragmentation. In panels (c) through (f), only the central regions are shown. The contours in each panel are for the surface density normalized by Σ_{\max} , whose value is given above each panel. Also given are the flux-to-mass ratio (Γ) at the density peak, dimensionless evolution time (t), and initial flux-to-mass ratio (Γ_0). The arrows are velocity vectors normalized by the effective isothermal sound speed c_s (without magnetic contribution), whose magnitude is indicated above each panel. Note that in panel (a) the added perturbation lowers the flux-to-mass ratio $\Gamma = 1.43$ from the reference value $\Gamma_0 = 1.5$ by 5%, corresponding to the fractional amplitude of the perturbation. For dimensional units, see subsection § 2.3.

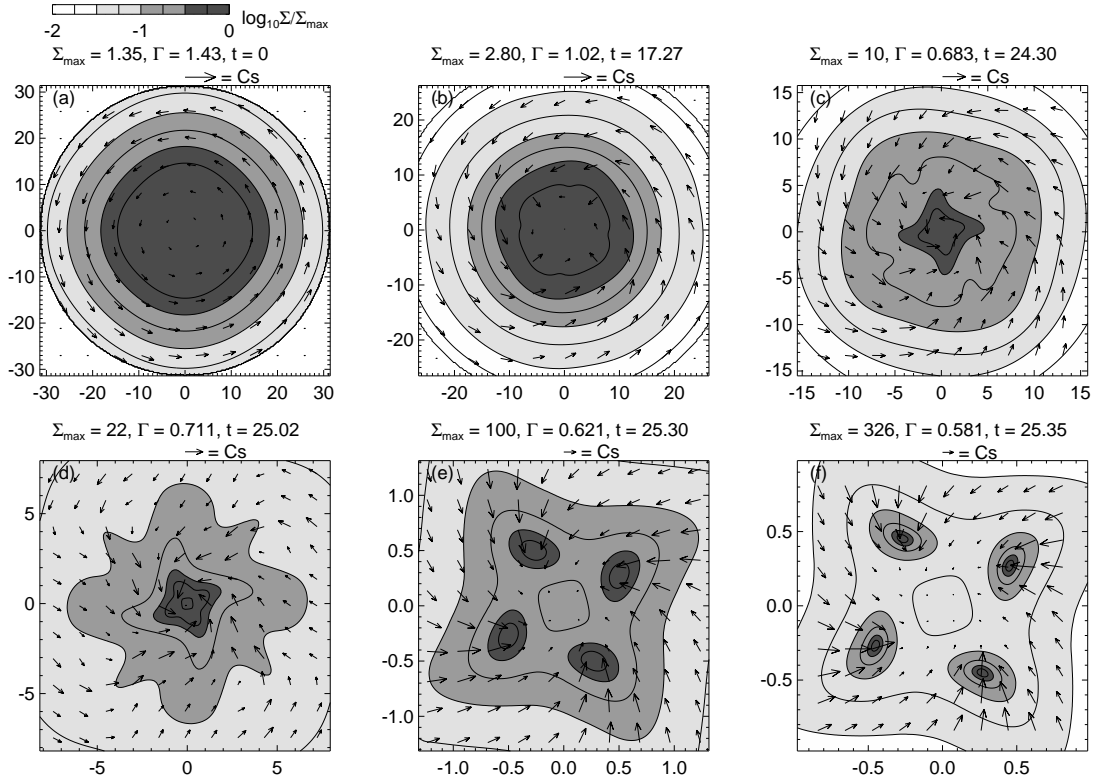


FIG. 2.— Snapshots of the surface density distribution and velocity field of the “standard” model with parameters $(r_0, n, \omega, \Gamma_0, A) = (5\pi, 8, 0.1, 1.5, 0.05)$, showing the growth of an $m = 4$ perturbation in a slowly-rotating cloud leading to fragmentation. The contours, arrows and notations have the same meaning as in Fig. 1.

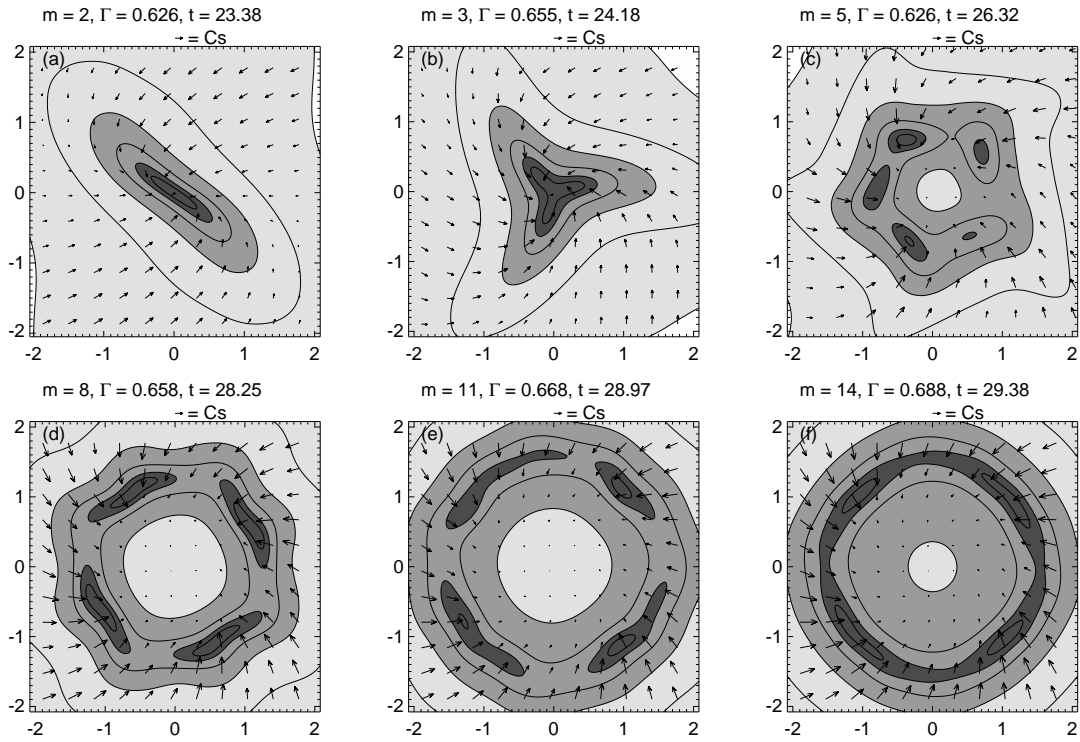


FIG. 3.— Snapshots of the surface density distribution and velocity field at a time corresponding to $\Sigma_{\max} = 10^2$ for the “standard” cloud perturbed by six selected modes of standard fractional amplitude $A = 0.05$. The imposed modes are $m = 2$ (a), 3 (b), 5 (c), 8 (d), 11 (e), and 14 (f). The contours and arrows have the same meaning as in Fig. 1, and the numbers above each panel denote the mode of perturbation (m), flux-to-mass ratio (Γ) at the density peak, and dimensionless evolution time (t). The connection between fragmentation and ring formation is evident.

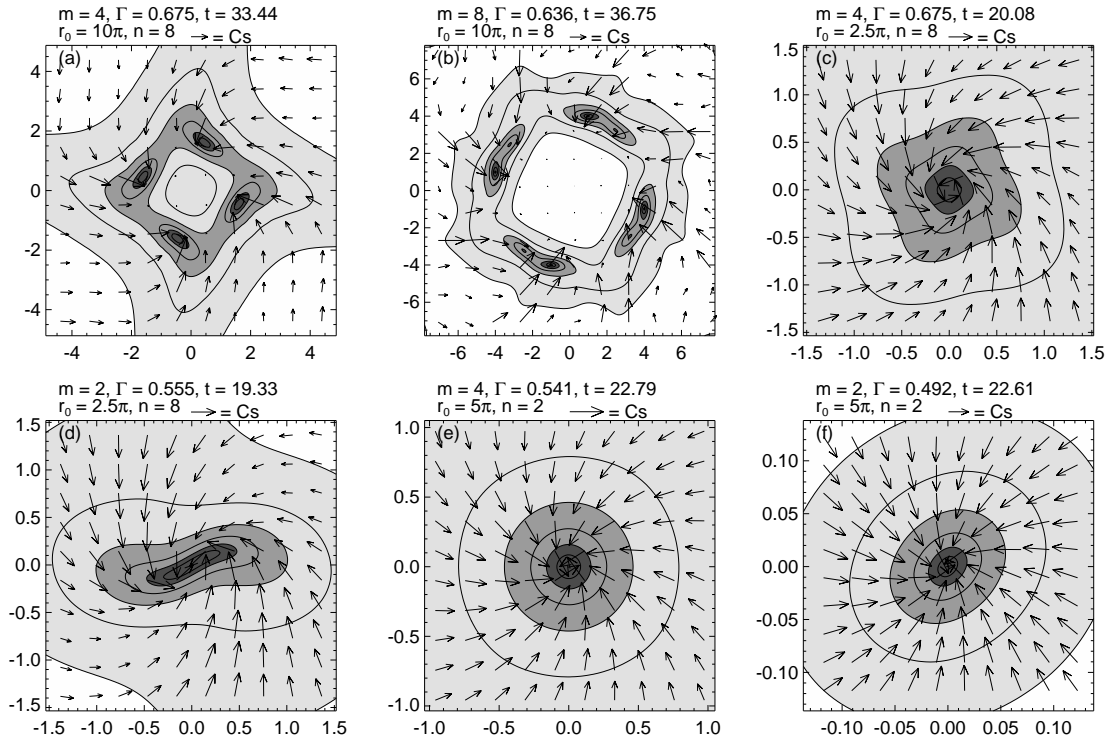


FIG. 4.— Snapshots of the evolution of three clouds at a time when $\Sigma_{\max} = 10^2$, showing the beneficial effects of a larger characteristic radius r_0 on cloud breakup (panels a and b), and the negative effects of a smaller r_0 (panels c and d) or n (more centrally peaked density distribution; panels e and f) on fragmentation and bar formation. The contours and arrows are the same as in Fig. 1. The models are specified by the numbers above each panel (see also Table 1).

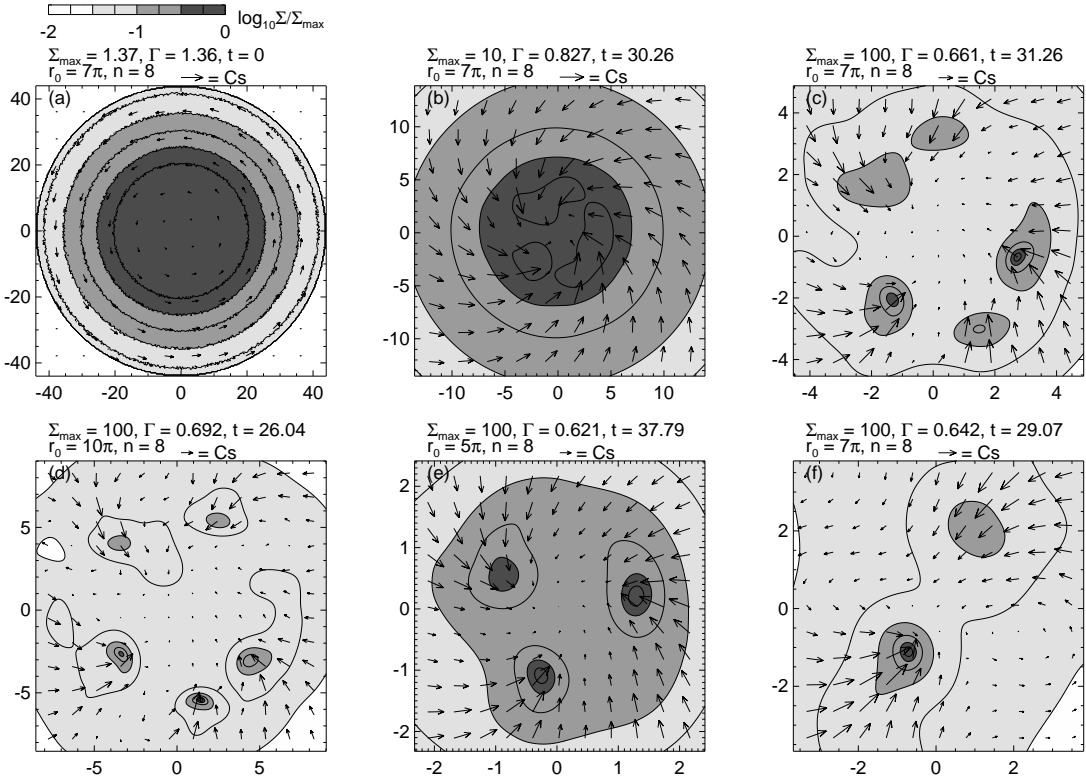


FIG. 5.— Snapshots showing the evolution and fragmentation of an $r_0 = 7\pi$ cloud in the presence of a random density perturbation of fractional amplitude $A = 0.1$ (panels a-c; the “canonical” model), and the effects of varying characteristic radius ($r_0 = 10\pi$ and 5π for panel d and e respectively) on the number of fragments obtained. In panel f), an $m = 2$ mode of very small fractional amplitude $A = 0.01$ is superposed on the random perturbation of the canonical model, leading to the production of a double-core, which may have implications for wide binary formation. The contours, arrows and notations have the same meaning as in Fig. 1 and other figures.